ROS-responsive capsules engineered from EGCG-Zinc networks improve therapeutic angiogenesis in mouse limb ischemia

Zuoguan Chen[a,1], Jianwei Duan[b,1], Yongpeng Diao[a], Youlu Chen[b], Xiaoyu Liang[b], Huiyang Li[b], Yuqing Miao[a], Qing Gao[a], Liang Gui[a], Xiaoli Wang[b], Jing Yang[b,*], Yongjun Li[a,**]

[a] Department of Vascular Surgery, Beijing Hospital, National Center of Gerontology, Institute of Geriatric Medicine. Chinese Academy of Medical Sciences and Peking Union Medical College. Graduate School of Peking Union Medical College, Beijing, 100730, PR China
[b] Tianjin Key Laboratory of Biomaterial Research, Institute of Biomedical Engineering, Chinese Academy of Medical Sciences and Peking Union Medical College, Tianjin, 300192, PR China

A B S T R A C T

The successful treatment of limb ischemia requires that promote angiogenesis along with microenvironment improvement. Zinc ions have been reported to stimulate angiogenesis, but application was limited to the toxicity concerns. We hypothesized that zinc based metal-EGCG capsule (EGCG/Zn Ps) can achieve sustained release Zn^{2+} resulting in reduced toxicity and improve angiogenesis as well as the improvement of microenvironment by ROS scavenging of EGCG. The surface morphology, zeta potential, infrared absorbance peaks and zinc ion release profile of the EGCG/Zn Ps were measured. In vitro, EGCG/Zn showed significantly antioxidant, anti-inflammatory and induced cell migration effect. In addition, EGCG/Zn Ps enabled the sustained release of zinc ions, which reduced cytotoxicity and enhanced the secretion of vascular endothelial growth factor (VEGF) in vitro *and* in vivo. In mouse models of limb ischemia, EGCG/Zn Ps promoted angiogenesis and cell proliferation in ischemic tissues. Moreover, EGCG/Zn Ps group exhibited the most significant recovery of limb ischemic score, limb temperature and blood flow than other groups. In conclusion, EGCG/Zn Ps is a safe and promising approach to combine the merit of Zn^{2+} and EGCG, thus enabling the direct application to limb ischemia.

1. Introduction

The prevalence of peripheral arterial disease (PAD) has markedly increased, affecting nearly 20% of people over 60 years of age [1]. Critical limb ischemia (CLI) is the most severe clinical manifestation of PAD, resulting in the chronic inadequate supply of oxygen and nutrients to the extremities [2,3]. CLI has become a major source of morbidity and mortality, which causes considerable economic and societal burdens. Despite various therapeutic strategies like surgical and endovascular revascularization, a substantial number of patients are not eligible for those treatments [4]. Therefore, therapeutic angiogenesis, which aims to revascularize the ischemic tissue via capillaries regeneration and artery out of existing vessels has been extensively studied. Currently, multiple growth factors and stem cells have been tried as an angiogenic promoter [5–7]. However, their clinical applications are limited due to their short half-life, poor stability, off-target effects,

high cost and overlook the harmful microenvironment of ischemic tissue [8,9]. The overexpressed H_2O_2 in ischemic muscles results in inflammatory responses and disturbs the promotion of angiogenesis by inhibiting the vascular endothelial growth factor (VEGF) expression [10,11]. Therefore, a efficacious, safe and cost-effective strategy that promote angiogenesis along with microenvironment amelioration is urgent to develop [12].

Epigallocatechin-3-gallate (EGCG) as the major polyphenol in green tea, has demonstrated the beneficial functions including ROS scavenging, antioxidation, anti-inflammatory, etc. [13,14] Hence, EGCG possess potential value for application in the improvement of limb ischemic microenvironment. In addition, EGCG could coordinate with many different metal ions to form metal-polyphenol networks (MPNs), which arouse numerous interest due to single-step formation, high biocompatibility and versatility [15–17]. Some MPNs were applied for anticancer drug delivery due to characteristic of ROS response [18,19].

Meanwhile, zinc ions have been reported to have the ability to promote angiogenesis, cell proliferation, and migration [20]. Moreover, its cellular and molecular mechanisms in modulating the wound healing process were reported in 2017 [21]. However, its application was limited because of the significant toxicity [22]. Therefore, the sustained and controlled release of zinc ions have attracted considerable attentions [23,24].

Herein, zinc based metal-EGCG capsules (referred as EGCG/Zn Ps) was synthesized through the coordination between EGCG and zinc ions, which could not only achieve sustained release of Zn^{2+} resulting in reduced toxicity and improved angiogenesis as well as the improvement of microenvironment by ROS scavenging of EGCG. In vitro, the effect of antioxidant, anti-inflammatory, promotion of cell migration and VEGF expression of EGCG/Zn Ps were evaluated. Besides, the effect of promoting angiogenesis, cell proliferation and the recovery of limb blood perfusion, temperature and ischemic score of EGCG/Zn Ps were assessed with the mouse model of limb ischemia.

2. Experimental section

2.1. Materials

Epigallocatechin-3-gallate (EGCG, 95%) was purchased from Dalian Meilun Biotech Co. Ltd (Dalian, China). $Zn(NO_3)_2 \cdot 6H_2O$ (99.0%), $CaCl_2$ and Na_2CO_3 were purchased from Tianjin Xindayu Chemical Co. Ltd (Tianjin, China). Hydrogen peroxide (H_2O_2, 30 wt%), poly (sodium. 4-styrenesulfonate) (PSS, MW ca. 70 000) were purchased from Tianjin Guangfu Fine Chemical Research Institute (Tianjin, China). 3-[4,5-dimethylthialzol-2-yl]-2,5-diphenyltetrazolium bromide (MTT) was purchased from Sigma-Aldrich. PBS, anhydrous dimethyl sulfoxide (DMSO, 99.9% purity), RPMI 1640 medium (Hyclone), DMEM-F12, endothelial cell growth medium, fetal bovine serum (FBS), Tween 20, LPS, PMA were purchased from Solarbio Science &Technology Co. Ltd (Beijing, China). 1,1-Diphenyl-2-picrylhydrazyl radical 2,2-Diphenyl-1-(2,4,6-trinitrophenyl) hydrazyl (DPPH free radical, product number: D4313) was purchased from Tokyo Chemical Industry Co. LTD. Transwell BD Matrigel was purchased from Corning Incorporated (New York, USA). Anti-mouse enzyme-linked immunosorbent assay (ELISA) kits, TNF-α, and IL-6 were purchased from eBioscience (San Diego, CA, USA). VEGF, CD31and HIF-1α antibody were obtained from Abcam (Cambridge, UK). PCNA was obtained from Santa Cruz Biotechnology Inc (CA, USA). All chemicals were used without further purification.

2.2. Cells and animals

NIH 3T3, RAW264.7 and HUVEC were purchased from the Cell Bank of China Academy of Sciences, and cultured according to the manufacture's guidelines. NIH 3T3 is one kind of mouse fibroblast cells and RAW264.7 is one kind of mouse macrophage cells. Six-week-old female Institute of Cancer Research mice were bought from the Academy of Military Medical Sciences (Beijing, China). All experimental procedures were approved by the Institutional Animal Care and Use Committee at Peking Union Medical College.

2.3. Synthesis of EGCG/Zn Ps

$CaCO_3$ particles were synthesized via a fast coprecipitation method [25]. Briefly, the stock solutions of $CaCl_2$ and Na_2CO_3 with a concentration of 20 mM were prepared and poly (sodium 4-styrene sulfonate) was added in the above solutions with a concentration of 1 mg mL^{-1} 10 mL of Na_2CO_3 stock solution was rapidly poured into 10 mL of $CaCl_2 \cdot 2H_2O$ stock solution with stirring for 30 s at room temperature. The resulting $CaCO_3$ microparticles were collected by centrifugation at 6010*g* for 5 min and washed three times with deionized water. Then, 0.5 mL of EGCG (24 mM) and 0.5 mL of $Zn(NO_3)_2 \cdot 6H_2O$ (24 mM) were successively added into 4 mL of $CaCO_3$

suspension. Thereafter, 5 mL of MOPS (100 mM, PH 8.0) buffer solution was added to adjust the suspension pH. The resulting particles were washed to remove excess EGCG and Zn^{2+}. The process of EGCG/Zn deposition was repeated three times, then $CaCO_3$ coated with EGCG/Zn layer were obtained. Finally, the $CaCO_3$ template was removed by immersing in EDTA solution (200 mM, PH = 8) for three minutes to obtain EGCG/Zn capsules. SEM images of EGCG/Zn Ps were performed. ICP and XPS were employed to detect the content of zinc element and the change of binding energy. A Nicolet Nexus 470-ESp FTIR spectrometer (Thermo Fisher Scientific, Waltham, MA, USA) was employed to analyse the main functional groups of EGCG and EGCG/Zn Ps.

2.4. In vitro Zn ions release

The release of Zn^{2+} from EGCG/Zn Ps in H_2O or H_2O_2 (pH 7.4, 37 °C) was assessed. Briefly, EGCG/Zn Ps (15 mg) samples were incubated in 5 mL H_2O or H_2O_2 (40 μM) with continuous shaking (100 rpm, 37 °C). At predetermined intervals, 1 mL of release medium was taken out and equal volume of fresh medium was replenished. The amount of released zinc was measured by inductively coupled plasma mass spectrometry.

2.5. Cytotoxicity of EGCG/Zn in vitro

The cytotoxicity was determined by MTT assay. NIH 3T3 and HUVEC were seeded in 96-well plates (5 × 10^3 cells per well) and incubated with varying concentrations of $Zn(NO_3)_2$ or EGCG/Zn Ps for 24 h. Then, MTT solution was added to each well (final concentration of 0.5 mg mL^{-1}) and incubated for an additional 4 h. After that, the medium was removed and 100 μL of DMSO was added. Absorbance at 570 nm was measured with a microplate reader. Cell viability was expressed as a percentage of absorbance between experiment and control group (n = 3).

2.6. In vitro and intracellular ROS scavenging activity

H_2O_2 scavenging abilities of EGCG, $Zn(NO_3)_2$, and EGCG/Zn Ps were carried out at room temperature with the Amplex Red assay. Pipet 50 μL of 40 μM H_2O_2 solution (PBS, 25 mM, pH 7.4) into individual wells of a 96-well microplate, and then 50 μL of EGCG, $Zn(NO_3)_2$ or EGCG/Zn Ps at different concentration was added. After reaction for 2 h, the H_2O_2 concentration was measured with the Amplex Red assay kit according to the manufacturer's protocol (Invitrogen, US). Besides, DPPH free radical scavenging of EGCG/Zn Ps was further evaluated. Firstly, different concentrations of EGCG/Zn Ps suspension were added into 2 mL of DPPH ethanol solution (100 μg mL^{-1}). Ethanol was used as control. After incubating for 30 min, the absorbance at 515 nm of above mixed solution supernatants was detected with a Varioskan Flash Microplate Reader (Thermo Fisher Scientific). As for intracellular ROS scavenging ability, HUEVC, NIH-3T3 and RAW-264.7 cells (4 × 10^5 cells) were seeded in a 24-well plate, then PMA was added into medium for up-regulating intracellular ROS level. Subsequently, different concentrations of EGCG/Zn Ps were added into medium. After incubating for 4 h, intracellular ROS level was detected by DCFH-DA, and the florescent images were obtained with a CLSM-410 (Zeiss, Jena, Germany). Besides, the fluorescence intensity of cells was quantifies with a BD Accuri C6 flow cytometer (BD Biosciences, San Jose, CA).

2.7. Anti-inflammatory, antioxidant, VEGF expression in vitro

RAW264.7 cells were seeded in 24-well plates (1 × 10^5 cells per well) and treated with LPS (1 μg/mL) or different concentration of EGCG/Zn Ps (10, 25, 50, 100, 200 and 400 μg/mL). And the cytokines in supernatants (IL-6 and TNF-α) were analyzed by ELISA. LPS was used as positive control and PBS was used as negative control. NIH 3T3 cells were seeded in 96-well plates (5 × 10^3 cells per well) and incubated
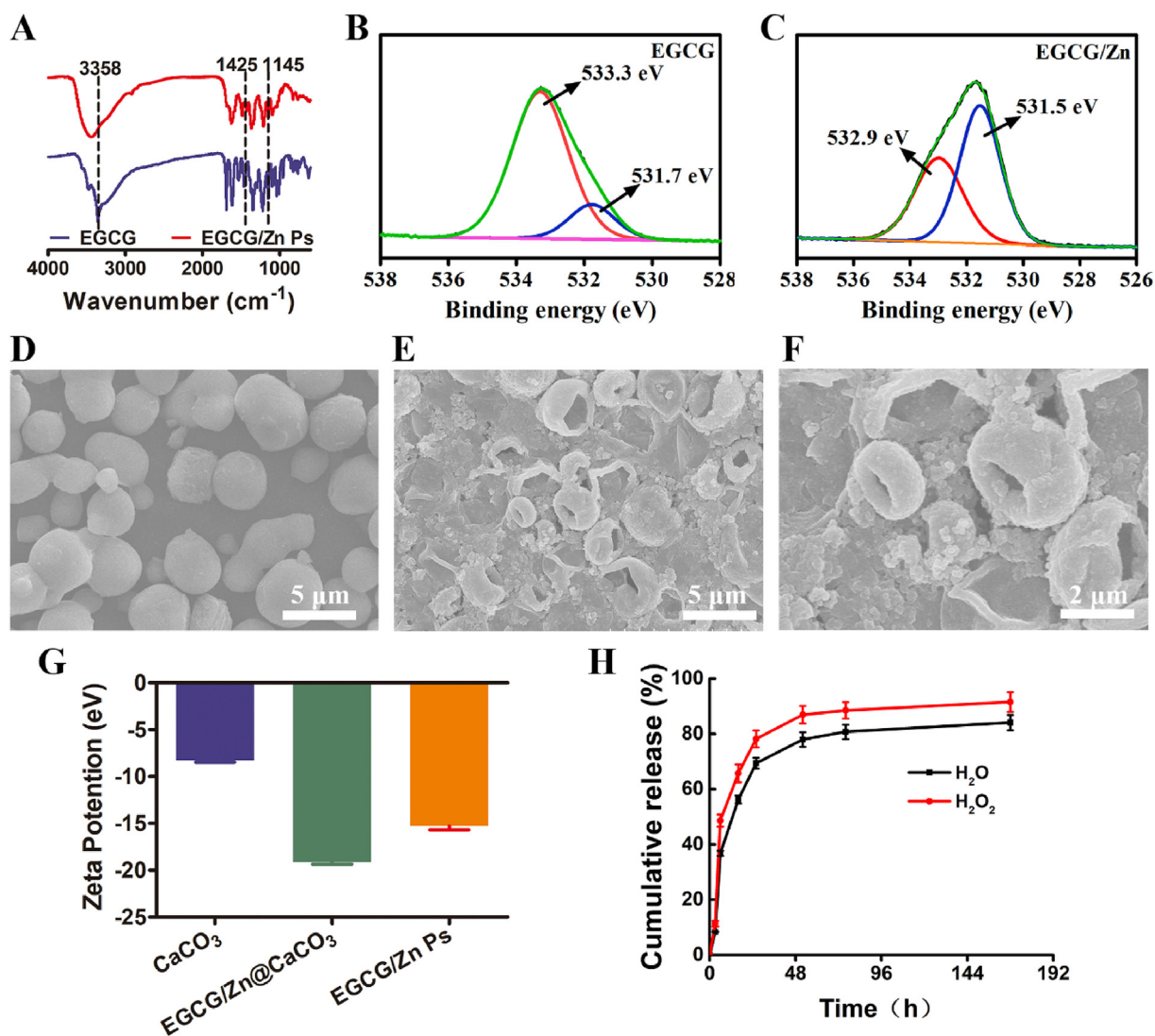
Fig. 1. The synthesis and characterization of EGCG/Zn Ps. (A) FTIR spectrometry of EGCG and EGCG/Zn Ps. The high-resolution O 1s XPS spectra of EGCG (B) and EGCG/Zn (C). SEM image of EGCG/Zn@CaCO$_3$ (D) and EGCG/Zn Ps (E, F). (G) The zeta potentials of CaCO$_3$, EGCG/Zn@CaCO$_3$ and EGCG/Zn Ps. (H) In vitro release of Zn^{2+} from EGCG/Zn Ps incubating in H$_2$O (pH 7.4) or H$_2$O$_2$ (40 μM). Values are mean ± SD (n = 3).

with medium containing 0.5 mM H$_2$O$_2$ as well as varying concentrations of EGCG/Zn Ps (25, 50, 100, 200 and 400 μg mL^{-1}) for 24 h. Finally, the cell viability of NIH 3T3 was detected by MTT assay. HUEVC were seeded into 24-well plates. After 24 h of growth (at ~80% confluency), the cells were treated with EGCG, Zn(NO$_3$)$_2$, or EGCG/Zn Ps for 12 h. The expression level of VEGF protein in the medium was measured with a commercially available ELISA kit (R&D systems). PBS was used as a negative control.

2.8. In vitro scratch assay and transwell migration assay

HUEVC and NIH 3T3 cells were seeded in 6-well plates (4 × 10^5 cells per well) and allowed to form a confluent monolayer. After starvation with serum free medium for 18 h, the cell monolayer was scratched in a straight-line with a 200 μL pipette tip to mimic an incisional wound. Subsequently, cell debris were washed away with PBS, and treated by Zn(NO$_3$)$_2$ with different concentrations of Zn ions (Zn^{2+}: 10, 25, 50, 100, and 200 μM) at 37 °C with the medium containing 1% FBS. At desired time intervals, the cells were photographed and the rate of cell migration was calculated.

According to above method, in vitro scratch assay was also performed by treating the cells with PBS, EGCG, Zn(NO$_3$)$_2$ (Zn^{2+}: 25 μM),

or EGCG/Zn Ps (Zn^{2+}: 25 μM), and the rate of cell migration was also calculated. Meanwhile, in vitro transwell migration assay was further performed. HUEVC cells (5 × 10^4/ml cells in 200 μL of ECM) were added to the upper chamber with PBS, EGCG, Zn(NO$_3$)$_2$ (Zn^{2+}: 25 μM), or EGCG/Zn Ps (Zn^{2+}: 25 μM). 1300 μL of ECM containing 20% FBS was added to the lower chamber, then cells were cultured with 5% CO$_2$ for 24 h at 37 °C. The cells were removed from the filter upper surface, fixed by methyl alcohol and stained with crystal violet for 15 min. On the underside of the filter, these cells that migrated through the filter pores were counted in 5 fields per insert and the average number of migrated cell was obtained. Three identical replicates were performed.

2.9. Establishment of left hindlimb ischemia animal model

The animal model of hindlimb ischemia was established according to our previously described methods [26]. Briefly, animals were anesthetized by intraperitoneal administration of chloral hydrate (400 mg/kg), and the hair on their limbs was completely removed with depilatory cream and wiped with ethanol. A skin incision parallel to the left inguinal ligament was made to allow for the proper isolation, ligation, and excision of the femoral artery from its origin just above the inguinal ligament to its bifurcation at the origin of the saphenous and
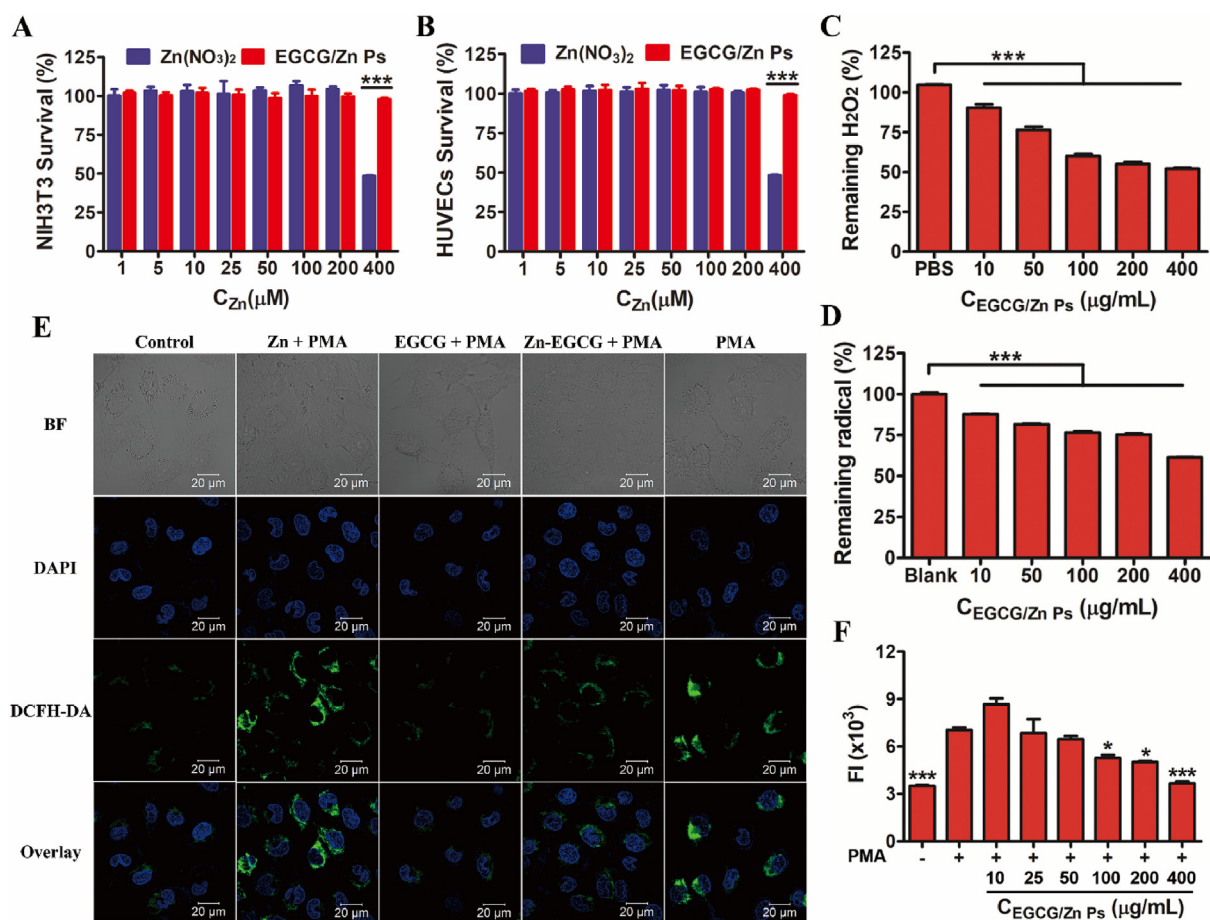
Fig. 2. Cytotoxicity evaluation and ROS-responsiveness of EGCG/Zn Ps. The cytotoxicity of $Zn(NO_3)_2$ and EGCG/Zn Ps to NIH 3T3 (A) and HUVEC (B). H_2O_2 (C) and free radical (D) scavenging by EGCG/Zn Ps. (E) CLSM images of ROS scavenging in HUVEC using DCFH-DA probe (EGCG/Zn Ps, 50 μg/mL). (F) Total fluorescence intensity (FI) of dichlorofluorescein fluorescence in HUVEC. The data are presented as the mean ± SD (n = 3, *P < 0.05, **P < 0.01, ***P < 0.001).

popliteal arteries. The incision was closed using 6-0 prolene sutures. On the first day after operation, the mice were randomly divided into four groups (n = 6), which were treated with PBS (40 μL), EGCG (40 μL, 17.05 μg/ml), $Zn(NO_3)_2 \cdot 6H_2O$ (40 μL, Zn^{2+}:25 μM), EGCG/Zn Ps (40 μL, Zn^{2+}:25 μM), respectively. The mice were treated three times, once every two days from the first day after operation. Each injection was performed smoothly over at least 15 s, and the needle was left in the tissues for at least 10 s to prevent back-leakage. The diagram of intramuscular injection can be seen in Fig. S1 and the gastrocnemius was collected for further analysis (Fig. S2).

2.10. Limb ischemic, temperature, blood flow and neovascularization assessment

At day 0, 1, 3, 5, 7, 10 and 14 after operation, limb morphology was visually scored to evaluate the degree of ischemia-induced damage. Ten grades were used to measure the degree of limb ischemic injury (Table S1, Supporting Information). Both limbs blood flow were evaluated by Laser Doppler perfusion imager (Moor Instruments, United Kingdom). Mean values of perfusion were calculated from the stored digital color-coded images. The blood flow level of the ischemic (left) limb was normalized to the non-ischemic (right) limb to avoid data variations caused by ambient light and temperature. Meanwhile, limbs temperature was also recorded by infrared thermal imaging system (FLIR E6 System, USA) and the temperature ratio of ischemic to normal hindlimbs was calculated. Besides, microcirculation imaging of mouse limb was demonstrated with Micro-CT (Quantum GX, PerkinElmer, USA). In addition, the mice were weighed during the experiment, and the optics

images of hindlimbs were acquired by a digital camera on day 3, 7 and 14 after operation.

2.11. Histopathology analysis

The mice were euthanized on day 14 after operation. Tissue samples of ischemic muscles were separated and fixed in 4% paraformaldehyde for 24 h, and 7 μm frozen sections were prepared. The sections were stained with hematoxylin-eosin (HE) for morphological analysis. Immunohistochemistry staining of CD31 (1:400 dilution), HIF-1α or PCNA were analyzed by counting 3 random high-power fields (magnification × 200) on an inverted light microscope. The results were expressed as the number of CD31-positive cells, HIF-1α positive cells or proliferating cell nuclear antigen (PCNA) positive cells per mm^2. Quantification of the results was performed by densitometry (Image-Pro Plus 6.0, NIH, USA). Besides, the biocompatibility of EGCG/Zn Ps in vivo was evaluated by detecting the level of IL-6, TNF-α in the serum and HE staining of main organs.

2.12. Real-time quantitative polymerase chain reaction (RT-PCR) and Western blot

Trizol reagent (Invitrogen, CA, USA) was used to extract the total RNA in leg muscle harvested from the sacrificed mice according to the manufacturer's instructions. Prior to reverse transcription, the total RNA was digested with RNase-free DNase (Invitrogen, CA, USA), and the quality was determined by ultraviolet Spectrophotometer analysis. The cDNA was synthesized from the total RNA template using reverse
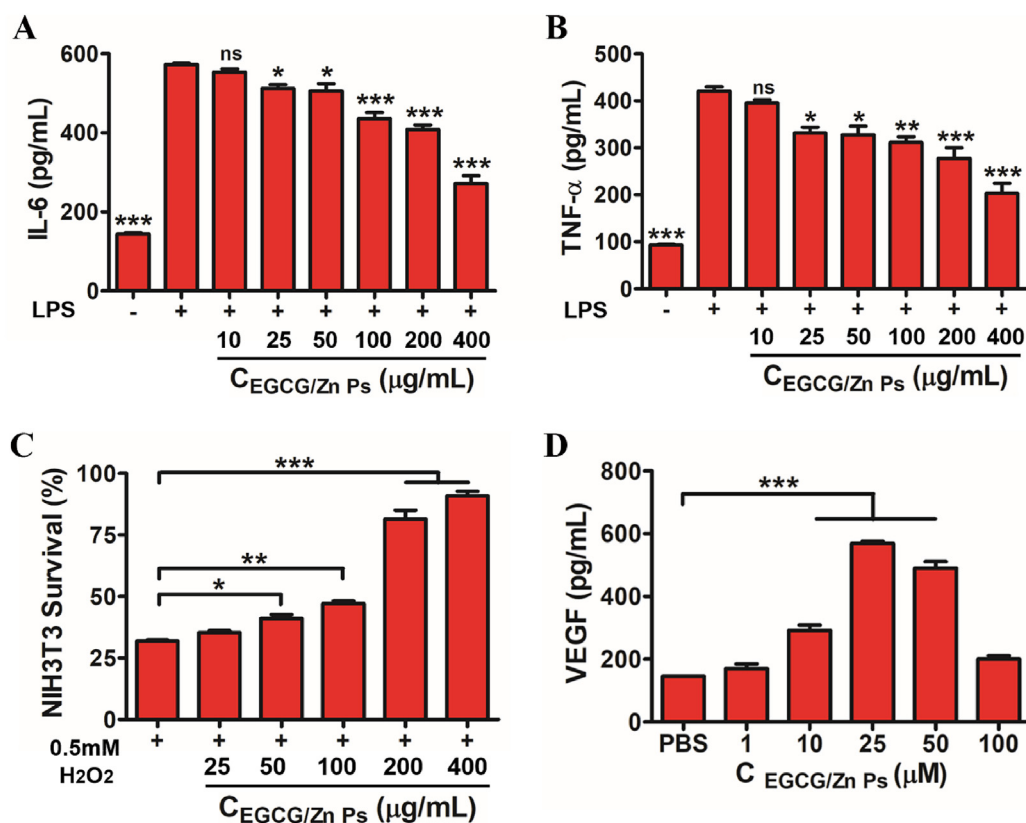
Fig. 3. Effect of EGCG/Zn Ps on different cells. The levels of IL-6 (A) and TNF-α (B) in the supernatant of RAW264.7 cells. (C) The NIH 3T3 cells survival detected by MTT assay. (D) The VEGF expression on HUVEC in response to EGCG/Zn Ps. The data are presented as the mean $\pm$ SD (n = 3, *P < 0.05, **P < 0.01, ***P < 0.001).

transcriptase (Invitrogen, CA, USA) and Olig (dT)12-18 primer (Promega, Germany). The conditions for PCR amplification were as follows: pre-denaturation at 95 °C for 10 min, 40 cycles of denaturation at 95 °C 15 s, annealing at 50 °C for 2 min, extention at 60 °C for 60 s. PCR products were purified with the Qiaquick DNA purification kit (Qiagen, Germany). The amplified products was detected using a sequence detection system (PE Applied Biosystem). Besides, protein samples were separated on SDS-polyacrylamide gels and then transferred to a polyvinylidene difluoride membranes, which were treated with blocking buffer (5% skim milk). Then the membranes were incubated with the primary antibody (anti-VEGF antibody) followed by incubation with an anti-mouse horseradish peroxidase conjugated secondary antibody. Immune reactivity was visualized using ECL plus system. Quantification of the results was performed by densitometry (Image J, NIH, USA) by comparing the density of identically sized areas (corresponding to immunoreactive bands) and total integrated density (arbitrary units).

2.13. Statistical analysis

Based on the normal distribution and equal variance assumption test, the data were expressed as mean $\pm$ standard deviation (SD) and analyzed via one-way analysis of variance (ANOVA) followed by Tukey's post-test analysis (GraphPad Prism 5, GraphPad Software, San Diego, USA). The differences were considered statistically significant at p < 0.05 (*), p < 0.01 (**) and p < 0.001 (***).

3. Results

3.1. Synthesis and characterization of EGCG/Zn Ps

The EGCG/Zn Ps were examined using Fourier transform infrared

(FTIR), X-ray photoelectron spectroscopy (XPS), Scanning electron microscope (SEM), Dynamic light scattering (DLS) and Inductively coupled plasma atomic emission spectroscopy (ICP-AES). FTIR spectra showed that the peaks at 1425 cm^{-1} and 1145 cm^{-1} of EGCG were buried and peak at 3358 cm^{-1} shifted to high wavenumber after zinc complexation (Fig. 1A). Besides, high resolution O1s XPS spectrum showed a major peak at 533.3 eV and a relatively small peak at 531.7 eV of EGCG shift to 532.9 eV and 531.5 eV, respectively (Fig. 1B and C). From Fig. 1D, SEM revealed that EGCG/Zn@CaCO$_3$ were spherical particle with smooth surface. After removing CaCO$_3$ template, the typical morphology of capsule's fold and creases were observed with an average diameter of 2–3 μm (Fig. 1E and F). DLS show that the surface zeta potential of CaCO$_3$ shifted from -8.3 ± 0.31 eV to -19.2 ± 0.35 eV after EGCG/Zn coordination layer formation, and then turn to -15.3 ± 0.7 eV after the removal of CaCO$_3$ template (Fig. 1G). Meanwhile, ICP revealed that the proportion of zinc ion increased from 1.8% in EGCG/Zn@CaCO$_3$ to 2.2%–8.8% in EGCG/Zn Ps. The sustained release of zinc ions from EGCG/Zn Ps were confirmed in H$_2$O or H$_2$O$_2$ solution. In the presence of H$_2$O$_2$, 78% and 92% of Zn ions were released within 26 h and 168 h, respectively, while only 69% and 84% of Zn ions were released incubating in H$_2$O solution (Fig. 1H). The accelerated release of Zn^{2+} from EGCG/Zn Ps was ascribed to the ROS responsivity of EGCG-zinc metal networks. All above changes of EGCG/Zn Ps were attributed to the coordination reaction between EGCG and Zinc ions.

3.2. The biocompatibility and ROS-responsiveness of EGCG/Zn Ps

As expected, EGCG/Zn Ps exhibited much lower cytotoxicity towards both NIH 3T3 and HUEVC cells at high zinc concentration (400 μM) (p < 0.001), indicating a better biocompatibility of EGCG/Zn Ps than Zn(NO$_3$)$_2$ (Fig. 2A and B). Fig. 2C and D suggested that H$_2$O$_2$
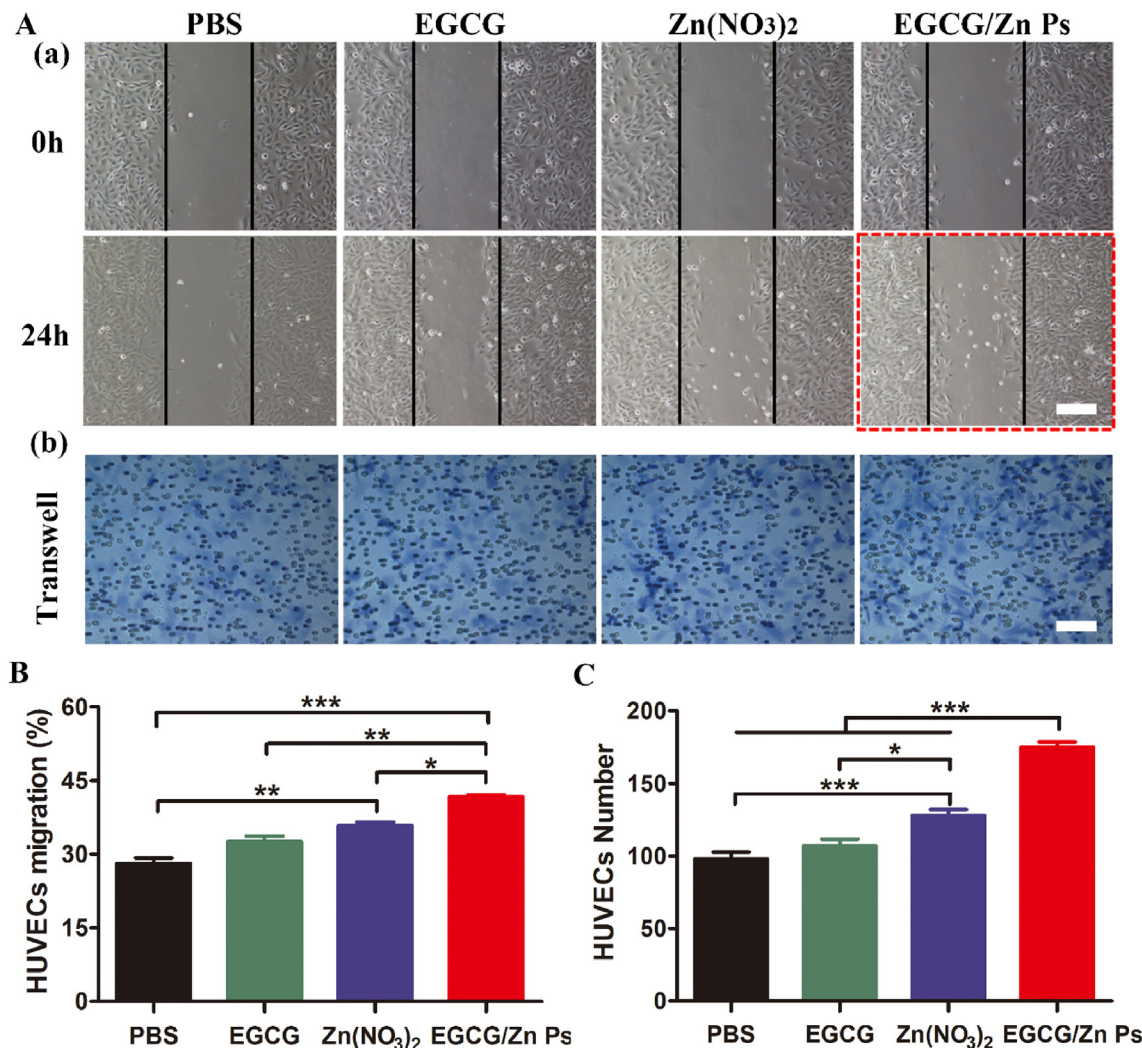
Fig. 4. The effects of EGCG/Zn Ps on HUVEC migration. (A) Digital images of HUVEC migration of (a) scratch assay and (b) transwell assay (Zn^{2+}, 25 μM). (B) Quantification of HUEVC migration by scratch assay. (C) Quantification of HUEVC migration by transwell assay. The data are presented as the mean ± SD (Scale bar: 50 μm; n = 3, *P < 0.05, **P < 0.01, ***P < 0.001).

or free radical could be effectively scavenged by EGCG/Zn Ps in a dose-dependent manner. EGCG/Zn Ps possess better H_2O_2 scavenging efficiencies than $Zn(NO_3)_2$ in all the investigated concentrations (Fig. S3). Meanwhile, intracellular ROS clearance was also detected by dichlorofluorescein diacetate (DCFH-DA). From confocal laser scanning microscopy (CLSM) images (Fig. 2E), an intense DCFA fluorescence signal implied that the intracellular ROS was obviously stimulated by propylene glycol monomethyl ether acetate (PMA) in human umbilical vein endothelial cells (HUVEC). While the DCFA fluorescence signal weaken due to intracellular ROS was eliminated by EGCG/Zn Ps. Similar results to HUVEC were also observed in NIH 3T3 and RAW264.7 (Figs. S4 and S5). Moreover, the capability of EGCG/Zn Ps obliterate intracellular ROS was further confirmed by flow cytometry in HUVEC (Fig. 2F).

3.3. Anti-inflammatory, antioxidant and VEGF expression in vitro

Compared with RAW264.7 cells unstimulated with LPS, the cells pulsed by lipopolysaccharide (LPS) showed high expression of pro-inflammatory cytokines IL-6 and tumor necrosis factor-α (TNF-α). Meanwhile, EGCG/Zn Ps exerted strong inhibitory effect on the secretion of TNF-α and IL-6 in a dose-dependent manner (Fig. 3A and B). Meanwhile, the antioxidant property of EGCG/Zn Ps was further confirmed by appraising the protection of NIH 3T3 from H_2O_2 toxicity. The

survival rate of NIH 3T3 cells incubating with 0.5 mM of H_2O_2 increased from 31.9% to 81.4% after adding 200 μg/mL of EGCG/Zn Ps (Fig. 3C). Besides, the VEGF expression on HUVEC induced by EGCG/Zn Ps was also evaluated (Fig. 3D). With the increasing concentration of EGCG/Zn Ps, the expression level of VEGF was increased but afterward decreased at the turning point of 25 μM. When incubating with 25 μM EGCG/Zn Ps, HUVEC manifested over 4-fold increase in the expression level of VEGF compared to phosphate buffered saline (PBS) control.

3.4. HUVEC migration

The optimal zinc ions concentration that stimulated cell migration without obviously cytotoxicity was determined via a scratch assay. As for HUVEC, $Zn(NO_3)_2$ at a concentration of 10 μM, 25 μM and 50 μM significantly enhanced cell migration, while $Zn(NO_3)_2$ at a concentration of 100 μM, 200 μM inhibited cell migration (Fig. S6). Therefore, the zinc ions concentration of 25 μM was chosen for all subsequent experiments. The effect of EGCG, $Zn(NO_3)_2$ and EGCG/Zn Ps on cell migration was also evaluated. PBS (20 μL) was used as the blank control. After incubation for 24 h, HUVEC exposed to EGCG-Zn Ps showed the highest migration (41.68 ± 2.46%), followed by those exposed to $Zn(NO_3)_2$ (35.86 ± 2.47%), EGCG (32.53 ± 2.04%), and PBS (28.12 ± 1.03%) (P < 0.0024; Fig. 4Aa, B). The HUVEC number migrating through the filter pores to the underside of the filter in the
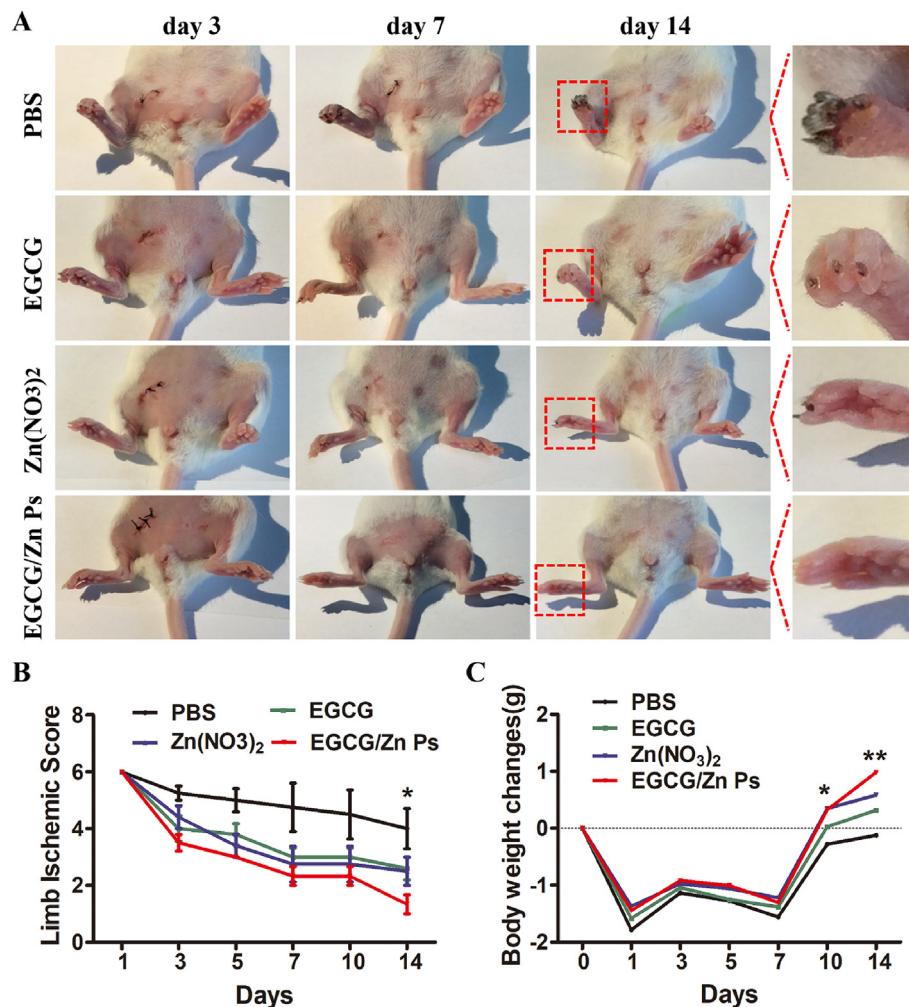
Fig. 5. The assessment of limb ischemic damage and body weight change of mouse. (A) Representative photographs of limbs. (B) Limb ischemic score over the time. (C) Body weight of the mice over the time. The data are presented as the mean $\pm$ SD (n = 6, *P < 0.05, **P < 0.01, * and ** are relative to all groups).

EGCG-Zn Ps group (237 $\pm$ 23) were significantly higher compared with the number in groups $Zn(NO_3)_2$ (176 $\pm$ 12), EGCG (143 $\pm$ 11) and PBS (116 $\pm$ 6) (P = 0.0003; Fig. 4Ab, C).

3.5. Therapeutic effects of EGCG/Zn Ps on hindlimb ischemia

The ischemia was confirmed by Laser Doppler perfusion imager (LDPI) after the femoral artery ligation surgery and limb ischemic scores of all mice were similar on day 1. However, on days 3, 7, 14 after operation, mice in PBS group suffered the most severe limb gangrene among all groups (Fig. 5A). Meanwhile, after operation, the ischemic score of mice in PBS group decreased more slowly compared with other groups. On day 14, the ischemic scores of mice in PBS, EGCG, $Zn(NO_3)_2$ and EGCG/Zn Ps groups were 4 $\pm$ 1.41, 2.6 $\pm$ 0.89, 2.5 $\pm$ 1 and 1.33 $\pm$ 0.58, respectively (P = 0.0395) (Figs. 5B and S7A). Meanwhile, although no significant difference on body weight change among four groups in the first week after operation, PBS group experienced the lowest recovery of body weigh on days 10 (P = 0.0092) (Fig. S7B). On day 14, the body weight changes of mice in PBS, EGCG, $Zn(NO_3)_2$ and EGCG/Zn Ps groups were −0.12 $\pm$ 0.15 g, 0.32 $\pm$ 0.27 g, 0.77 $\pm$ 0.25 g and 0.99 $\pm$ 0.12 g, respectively (P = 0.0014) (Fig. 5C, Fig. S7C).

The limb blood flow was monitored in vivo by LDPI at day 1, 3, 5, 7, 10 and 14 (Fig. 6A). Preoperatively, the blood flow ratio between the two normal hindlimbs for all mice was set to 1.0. On day 1, the blood flow ratio between the ischemic and normal limb was similar among all

the groups. Subsequently, the blood flow ratio slowly recovered over time and mice in EGCG/Zn Ps group exhibited the quickly recovery of blood flow ratio (Fig. 6A, C). On day 14, the blood flow ratio in PBS, EGCG, $Zn(NO_3)_2$ and EGCG/Zn Ps groups were 0.772 $\pm$ 0.057, 0.789 $\pm$ 0.048, 0.824 $\pm$ 0.0185 and 0.869 $\pm$ 0.445, respectively (P = 0.0003) (Fig. 6C). Similar tendency of limb temperature change were confirmed by infrared thermal imaging system (Figs. S8A and B). Moreover, we furthermore evaluated vessel volume of limb ischemia by Micro-CTA on days 14. The vessel volume in PBS, EGCG, $Zn(NO_3)_2$ and EGCG/Zn Ps groups were 32.41 $\pm$ 1.106, 35.17 $\pm$ 1.070, 40.42 $\pm$ 1.149 and 47.43 $\pm$ 0.226, respectively (P = 0.0156) (Fig. 6B,D). Taken together, these results indicate that EGCG/Zn Ps is effective for repairing limb ischemia and augmenting structural neo-vascularization.

3.6. Angiogenesis and cell proliferation in vivo promoted by EGCG/Zn Ps

On day 14, HE staining of the muscle tissue suggested that mice in PBS group showed more serious atrophy in the gastrocnemius muscles than other groups (Fig. 7A). Immunohistochemistry staining indicated that significantly larger number of PCNA positive cells were observed in EGCG/Zn Ps group (0.559 $\pm$ 0.125) compared with PBS group (0.181 $\pm$ 0.064) (P < 0.001) (Fig. 7A and B), which indicated cells proliferation and tissue repair was facilitated. As for angiogenesis indicator, the CD31-positive cells in the PBS, EGCG, $Zn(NO_3)_2$, and EGCG/Zn Ps groups were 0.047 $\pm$ 0.011, 0.101 $\pm$ 0.025,
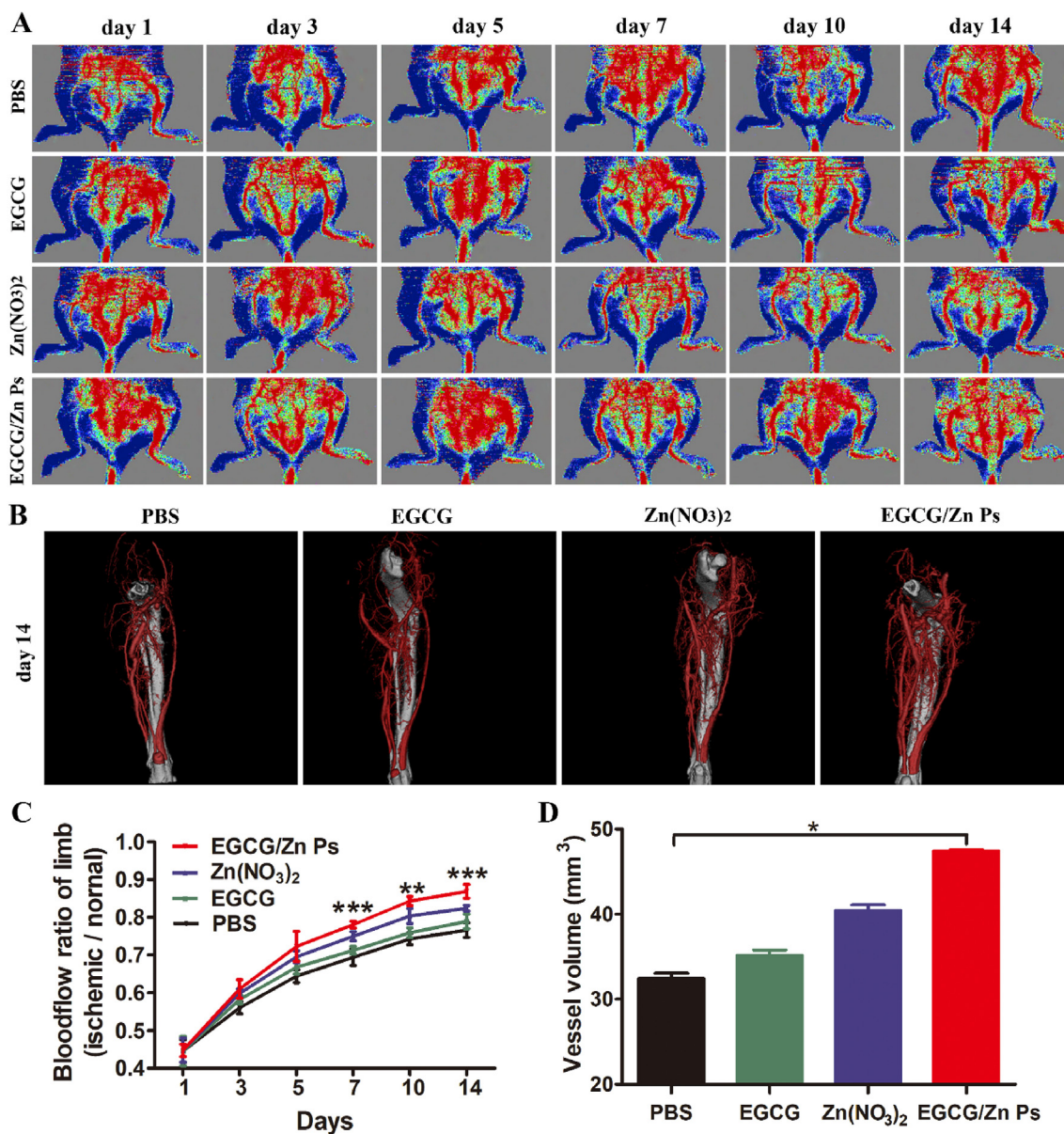
Fig. 6. Limb blood flow and neovascularization assessment. LDPI images (A) and quantitative (C) showed blood flow of limbs (n = 6, **P < 0.01, ***P < 0.001, ** and *** are relative to all groups). Micro-CTA images (B) and quantitative (D) showed vascular density. The data are presented as the mean ± SD (n = 3, *P < 0.05).

0.197 ± 0.007, and 0.271 ± 0.009, respectively (P < 0.001) (Fig. 7A, C).

3.7. HIF-1α and VEGF expression in vivo promoted by EGCG/Zn Ps

Meanwhile, HIF-1α positive cells were significantly higher in EGCG/Zn Ps group (0.119 ± 0.008) and Zn(NO₃)₂ group (0.116 ± 0.011) when compared with that in PBS group (0.074 ± 0.009) and EGCG group (0.068 ± 0.006) (P = 0.007) (Fig. 8A,C), which demonstrated that zinc ions could improve the expression of HIF-1α. Western blot analysis showed that the expression level of VEGF protein was obviously increased in EGCG/Zn Ps group (Fig. 8B), which up to 1.986 ± 0.304-fold over PBS group (P = 0.007) (Fig. 8D). The expression levels of VEGF mRNA in EGCG/Zn Ps, Zn (NO₃)₂ and EGCG group were 2.897 ± 0.752, 2.099 ± 0.429, and 1.357 ± 0.260-fold than that in PBS group, respectively (P = 0.0096) (Fig. 8E).

3.8. Biocompatibility of EGCG/Zn Ps in vivo

To determine the potential cumulative toxic effects of zinc ions, the toxicity of EGCG/Zn Ps to normal organ was evaluated. There was no significant histological evidence of accumulated toxicity in different organs associated with the administration of EGCG/Zn Ps (Fig. S9A). In addition, the pro-inflammatory cytokines (TNF-α and IL-6) in serum were also measured, the results showed that no significant abnormalities were observed in EGCG/Zn Ps group (Figs. S9B and C). These observations demonstrated that the cumulative toxicity of EGCG/Zn Ps in vivo can be negligible.

4. Discussion

The previous studies indicate that the 3′-OH–4′-OH moieties are the most likely binding sites of the polyphenols for metals [27]. In order to verify the successful coordination between EGCG and zinc in this EGCG/Zn Ps delivery system, several different detection methods, such
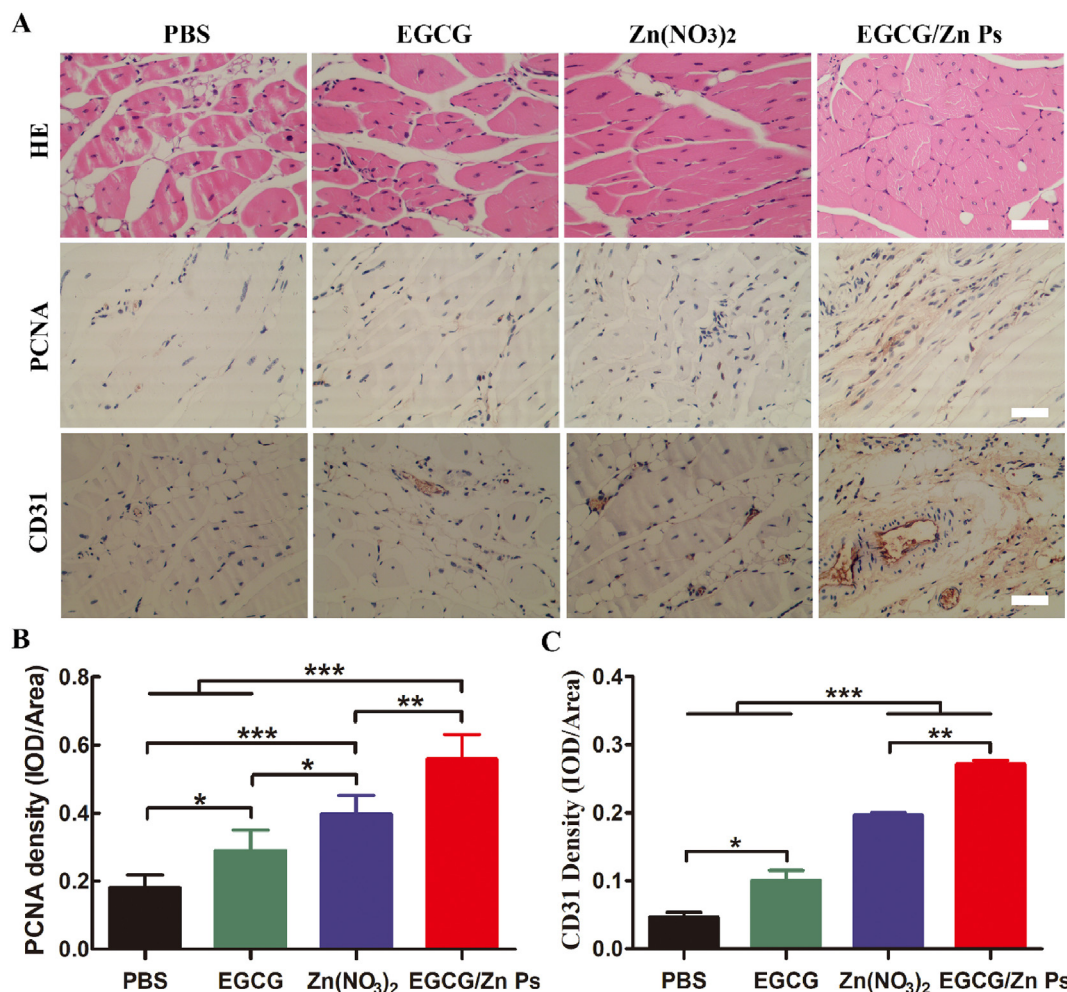
Fig. 7. Histological analysis (x200). (A) HE staining and immunohistochemical staining (PCNA and CD31) of ischemic muscles. (B) The quantification of PCNA positive cells. (C) The quantification of CD31-positive endothelial cells. (Scale bar: 100 μm; n = 3, *P < 0.05, **P < 0.01, ***P < 0.001).

as FTIR, XPS were adopted, which were strongly recommended by literatures [15,28]. First, the acidic nature of the galloyl groups in EGCG cause zeta potential shift between EGCG and zinc. Second, FTIR show the peaks at 1425 cm^{-1} and 1145 cm^{-1} were attributed to the saturated phenolic hydroxyl group of EGCG, which were buried in the EGCG/Zn Ps indicating the phenolic groups coordinated with metal ions. Third, the peak at 533.3 eV and 531.7 eV were corresponded to HO–C and C=O groups of EGCG [28]. After chelation with zinc ions, the O1s peak corresponding to the HO–C group shifted from 533.3 eV to lower binding energy of 532.9 eV, which suggested electron transfer from zinc ions to EGCG [29]. All these results were in accordance to the previous reports that the iron shift between phenolic and metals [16,28]. From our data, the release speed is a bit rapider in H$_2$O$_2$ than PBS, which may indicate that EGCG was oxidized by H$_2$O$_2$ to form benzoquinone species and the capsule decomposed consequently. Therefore, the mechanism of the Zn^{2+} release may due to the degradation of EGCG/Zn Ps. Besides, CaCO$_3$ was selected as the temporary template for its good biocompatibility.

As excess of extracellular Zn^{2+} is toxic, which could induce cell death [30]. Our findings were generally consistent with previous studies that the toxic concentration of Zn^{2+} various from 100 μM to 600 μM for different cells [31,32]. Meanwhile, compared to Zn(NO$_3$)$_2$, EGCG/Zn Ps showed much lower toxicity and better cell migration and VEGF expression, which was mainly attributed to the sustained release of zinc ions. Zn^{2+} has been reported to promote the expression of vascular endothelial growth factor (VEGF) [33]. Sustained release ion could exert better property with less toxic [34,35]. Besides, EGCG was

reported to accelerate reepithelialization and angiogenesis [36–38]. Therefore, it may be reasonable to explain that the EGCG/Zn Ps could exert the better result by combining the advantages of EGCG and Zn^{2+} sustain-release. In intro experiment, EGCG/Zn Ps has also been proved exerting antioxidant by eliminating H$_2$O$_2$ and showed a dose-dependent effect in the suppression of TNF-α and IL-6 expressions. These results were in accordance to previous studies [21,39].

The concentration of zinc to exert angiogenesis in the mouse model of limb ischemic is less well known. Attia reported that 30 μM of zinc-containing fluid had significantly improve the wound healing [40]. According to our in vitro experiment, the optimum concentration of zinc ions for cell migration and VEGF expression was 25 μM. So that 25 μM was chosen for in vivo study. Meanwhile, the injection interval of 1, 3 and 5 days were adopted for following two reason. First, the ROS level increased most obviously in the early stage of limb acute ischemia, so that is the best time for EGCG/Zn Ps to improvement the microenvironment [41]. Second, according to the release kinetic test, there was around 80% zinc ions release within the first 48 h and interval injection benefit to guarantee the dynamic stability of the zinc concentration. Besides, 14-day time point was selected because the angiogenesis was shown to be transient as blood vessels regressed with time [42]. It would be more valuable if we could demonstrate that the newly formed blood vessels are indeed mature and remain functional for more long time, but we mainly focus on demonstrating that EGCG/Zn Ps could exert angiogenesis in the present study. Long-term exploration worth further investigate.

Pipinos et al. reported that a high level of ROS generated in the
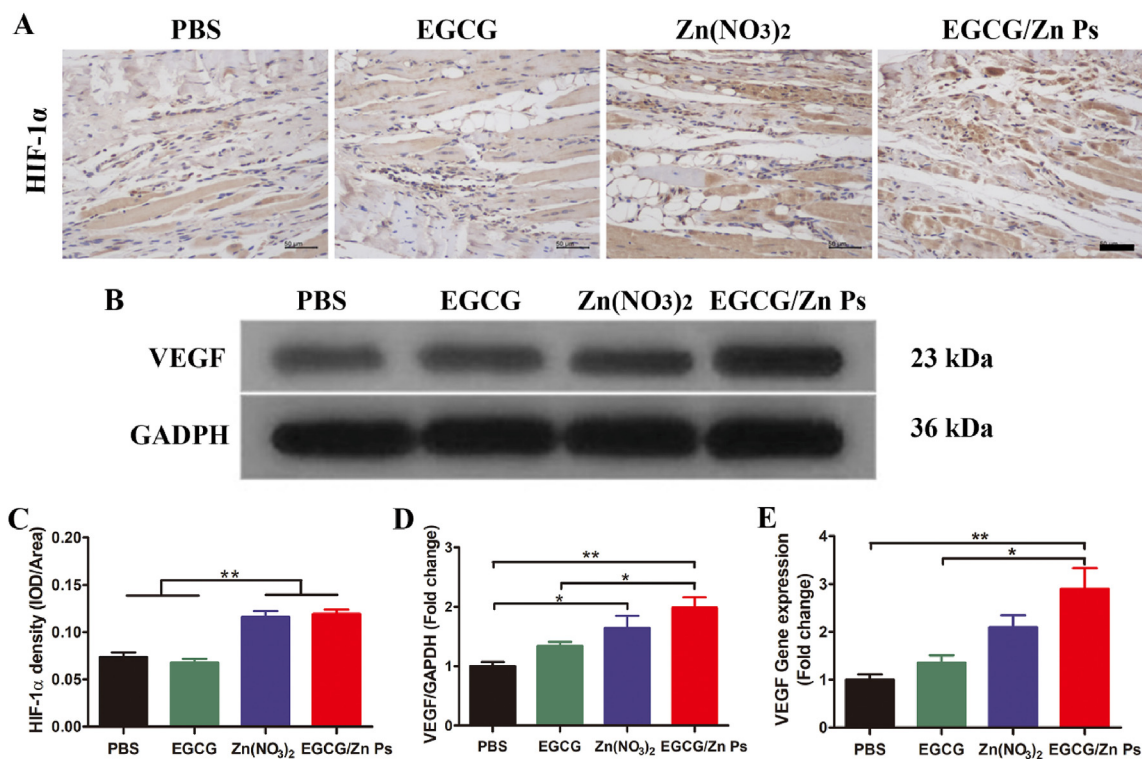
Fig. 8. HIF-1α and VEGF expression in vivo. (A) HIF-1α staining of ischemic muscles. (B) Western blot analysis result of VEGF expression. (C) The quantification of HIF-1α positive cells. (D) The expression level of VEGF protein expression. (E) The expression level of VEGF mRNA analyzed by PCR. The data are presented as the mean $\pm$ SD (Scale bar: 50 μm; n = 3, *$P < 0.05$, **$P < 0.01$, ***$P < 0.001$).

ischemia hindlimb causes oxidative stress that contributes to inflammation in PAD and suppresses angiogenesis [43]. Kwon reported that H_2O_2-responsive antioxidant polymeric nanoparticles as therapeutic agents for peripheral arterial disease [44]. Therefore, reduce ROS stress might be a promising approach to promote angiogenesis and relieve symptoms of ischemia [45,46]. Urao N has reported that angiogenesis and recovery of blood perfusion required an appropriate range of ROS because both too much and too little ROS were detrimental to cell viability and functions [47]. Therefore, in our study, no obvious ischemia improvement was observed from EGCG group, which might due to excessively clear of ROS. However, EGCG/Zn Ps enable to eliminate ROS in a more moderate way and keep ROS in proper level benefit for angiogenesis. In addition, our study confirmed that zinc could promote the expression of the hypoxia response factor HIF-1α, in accordance with previous reports [48], which was surely benefit from the sustained release of the EGCG/Zn Ps system. Therefore, it is reasonable that EGCG/Zn Ps could significantly improve angiogenesis in vivo, which were widely demonstrated by limb ischemic score, limb temperature, histological results as well as LDPI and micro-CTA evaluation. Certainly, more deeper mechanism worth further study.

5. Conclusion

EGCG/Zn Ps, a new delivery system with angiogenesis property, was developed based on green tea polyphenol–metal networks. The biocompatible EGCG/Zn Ps could not only achieve sustained release of Zn^{2+} resulting in reduced toxicity and enhancive angiogenesis but also improve microenvironment by scavenging excess ROS and inhibiting inflammatory cytokine via EGCG. Moreover, this study demonstrate a safe and promising approach to combine the merit of Zn^{2+} and EGCG, thus enabling it as a potential medical therapy to treat CLI.

Authorship contribution statement

Zuoguan Chen: Conceptualization, Methodology, Writing - original draft. **Jianwei Duan:** Conceptualization, Methodology, Writing - original draft. **Yongpeng Diao:** Funding acquisition, Writing - original draft. **Youlu Chen:** Methodology, Formal analysis. **Xiaoyu Liang:** Methodology, Formal analysis. **Huiyang Li:** Methodology, Formal analysis. **Yuqing Miao:** Software, Formal analysis. **Qing Gao:** Software, Formal analysis. **Liang Gui:** Software, Formal analysis. **Xiaoli Wang:** Funding acquisition, Formal analysis. **Jing Yang:** Funding acquisition, Writing - review & editing. **Yongjun Li:** Funding acquisition, Writing - review & editing, Supervision.

Declaration of competing interest

The authors declare that they have no known competing financial interests or personal relationships that could have appeared to influence the work reported in this paper.

Appendix A. Supplementary data

Supplementary data to this article can be found online at https://doi.org/10.1016/j.bioactmat.2020.07.013.

References

[1] N.M. Malyar, E. Freisinger, M. Meyborg, F. Luders, T. Furstenberg, K. Kroger, G. Torsello, H. Reinecke, Low rates of revascularization and high in-hospital mortality in patients with ischemic lower limb amputation: morbidity and mortality of ischemic amputation, Angiology 67 (2016) 860–869, https://doi.org/10.1177/0003319715626849.

[2] S. Elsayed, L.C. Clavijo, Critical limb ischemia, Cardiol. Clin. 33 (2015) 37–47, https://doi.org/10.1016/j.ccl.2014.09.008.

[3] L. Norgren, W.R. Hiatt, J.A. Dormandy, M.R. Nehler, K.A. Harris, F.G. Fowkes, K. Bell, J. Caporusso, I. Durand-Zaleski, K. Komori, et al., Inter-society consensus for the management of peripheral arterial disease (TASC II), Eur. J. Vasc. Endovasc. Surg. 33 (Suppl 1) (2007) S1–S75, https://doi.org/10.1016/j.ejvs.2006.09.024.

[4] N. Falluji, D. Mukherjee, Critical and acute limb ischemia: an overview, Angiology 65 (2014) 137–146, https://doi.org/10.1177/0003319712470966.

[5] J. Tongers, J.G. Roncalli, D.W. Losordo, Therapeutic angiogenesis for critical limb ischemia: microvascular therapies coming of age, Circulation 118 (2008) 9–16, https://doi.org/10.1161/circulationaha.108.784371.

[6] R. Forster, A. Liew, V. Bhattacharya, J. Shaw, G. Stansby, Gene therapy for peripheral arterial disease, Cochrane Database Syst. Rev. 10 (2018) Cd012058, , https://doi.org/10.1002/14651858.CD012058.pub2.

[7] M. Rigato, M. Monami, G.P. Fadini, Autologous cell therapy for peripheral arterial disease: systematic review and meta-analysis of randomized, nonrandomized, and noncontrolled studies, Circ. Res. 120 (2017) 1326–1340, https://doi.org/10.1161/circresaha.116.309045.

[8] O. Osipova, S. Saaya, A. Karpenko, S. Zakian, E. Aboian, Cell therapy of critical limb ischemia-problems and prospects, Vasa (2019) 1–11, https://doi.org/10.1024/0301-1526/a000787.

[9] D. Smadja, J.S. Silvestre, B.I. Levy, [Genic and cellular therapy for peripheral arterial diseases], Transfus. Clin. Biol. 20 (2013) 211–220, https://doi.org/10.1016/j.tracli.2013.02.026.

[10] A. Naldini, F. Carraro, Role of inflammatory mediators in angiogenesis, Curr. Drug Targets - Inflamm. Allergy 4 (2005) 3–8, https://doi.org/10.2174/1568010053622830.

[11] C.C. Chua, R.C. Hamdy, B.H. Chua, Upregulation of vascular endothelial growth factor by H2O2 in rat heart endothelial cells, Free Radic. Biol. Med. 25 (1998) 891–897, https://doi.org/10.1016/s0891-5849(98)00115-4.

[12] W. Jiang, D. Rutherford, T. Vuong, H. Liu, Nanomaterials for treating cardiovascular diseases: a review, Bioact. Mater. 2 (2017) 185–198, https://doi.org/10.1016/j.bioactmat.2017.11.002.

[13] B.N. Singh, S. Shankar, R.K. Srivastava, Green tea catechin, epigallocatechin-3-gallate (EGCG): mechanisms, perspectives and clinical applications, Biochem. Pharmacol. 82 (2011) 1807–1821, https://doi.org/10.1016/j.bcp.2011.07.093.

[14] Y.C. Shin, D.M. Shin, E.J. Lee, J.H. Lee, J.E. Kim, S.H. Song, D.Y. Hwang, J.J. Lee, B. Kim, D. Lim, et al., Hyaluronic acid/PLGA core/shell fiber matrices loaded with EGCG beneficial to diabetic wound healing, Adv. Healthc. Mater. 5 (2016) 3035–3045, https://doi.org/10.1002/adhm.201600658.

[15] J. Guo, Y. Ping, H. Ejima, K. Alt, M. Meissner, J.J. Richardson, Y. Yan, K. Peter, D. von Elverfeldt, C.E. Hagemeyer, et al., Engineering multifunctional capsules through the assembly of metal-phenolic networks, Angew Chem. Int. Ed. Engl. 53 (2014) 5546–5551, https://doi.org/10.1002/anie.201311136.

[16] H. Ejima, J.J. Richardson, K. Liang, J.P. Best, M.P. van Koeverden, G.K. Such, J. Cui, F. Caruso, One-step assembly of coordination complexes for versatile film and particle engineering, Science 341 (2013) 154–157, https://doi.org/10.1126/science.1237265.

[17] Q.Z. Zhong, S. Pan, M.A. Rahim, G. Yun, J. Li, Y. Ju, Z. Lin, Y. Han, Y. Ma, J.J. Richardson, et al., Spray assembly of metal-phenolic networks: formation, growth, and applications, ACS Appl. Mater. Interfaces 10 (2018) 33721–33729, https://doi.org/10.1021/acsami.8b13589.

[18] X. Wang, X. Li, X. Liang, J. Liang, C. Zhang, J. Yang, C. Wang, D. Kang, H. Sun, ROS-responsive capsules engineered from green tea polyphenol-metal networks for anticancer drug delivery, J. Mater. Chem. B 6 (2018), https://doi.org/10.1039/c7tb02688a 993-1120.

[19] Y. Ping, J. Guo, H. Ejima, X. Chen, J.J. Richardson, H. Sun, F. Caruso, pH-responsive capsules engineered from metal-phenolic networks for anticancer drug delivery, Small 11 (2015) 2032–2036, https://doi.org/10.1002/smll.201403343.

[20] Y. Song, H. Wu, Y. Gao, J. Li, K. Lin, B. Liu, X. Lei, P. Cheng, S. Zhang, Y. Wang, et al., Zinc silicate/nano-hydroxyapatite/collagen scaffolds promote angiogenesis and bone regeneration via the p38 MAPK pathway in activated monocytes, ACS Appl. Mater. Interfaces (2020), https://doi.org/10.1021/acsami.0c00470.

[21] P.H. Lin, M. Sermersheim, H. Li, P.H.U. Lee, S.M. Steinberg, J. Ma, Zinc in wound healing modulation, Nutrients 10 (2017), https://doi.org/10.3390/nu10010016.

[22] Z. Neščáková, K. Zheng, L. Liverani, Q. Nawaz, D. Galusková, H. Kaňková, M. Michálek, D. Galusek, A.R. Boccaccini, Multifunctional zinc ion doped sol - gel derived mesoporous bioactive glass nanoparticles for biomedical applications, Bioact. Mater. 4 (2019) 312–321, https://doi.org/10.1016/j.bioactmat.2019.10.002.

[23] J.J.D. Venezuela, S. Johnston, M.S. Dargusch, The prospects for biodegradable zinc in wound closure applications, Adv. Healthc. Mater. 8 (2019) e1900408, , https://doi.org/10.1002/adhm.201900408.

[24] K. Xing, R. Fan, F. Wang, H. Nie, X. Du, S. Gai, P. Wang, Y. Yang, Dual-stimulus-triggered programmable drug release and luminescent ratiometric pH sensing from chemically stable biocompatible zinc metal-organic framework, ACS Appl. Mater.

[25] Interfaces 10 (2018) 22746–22756, https://doi.org/10.1021/acsami.8b06270.

[25] Y. Wang, Y.X. Moo, C. Chen, P. Gunawan, R. Xu, Fast precipitation of uniform CaCO3 nanospheres and their transformation to hollow hydroxyapatite nanospheres, J. Colloid Interface Sci. 352 (2010) 393–400, https://doi.org/10.1016/j.jcis.2010.08.060.

[26] L. Wang, Z. Chen, Y. Li, J. Yang, Y. Li, Optical coherence tomography angiography for noninvasive evaluation of angiogenesis in a limb ischemia mouse model, Sci. Rep. 9 (2019) 5980, https://doi.org/10.1038/s41598-019-42520-3.

[27] R.F. de Souza, W.F. De Giovani, Synthesis, spectral and electrochemical properties of Al(III) and Zn(II) complexes with flavonoids, Spectrochim. Acta Mol. Biomol. Spectrosc. 61 (2005) 1985–1990, https://doi.org/10.1016/j.saa.2004.07.029.

[28] X. Huang, X. Liao, B. Shi, Hg(II) removal from aqueous solution by bayberry tannin-immobilized collagen fiber, J. Hazard Mater. 170 (2009) 1141–1148, https://doi.org/10.1016/j.jhazmat.2009.05.086.

[29] X. Huang, M. Gao, X. Liao, B. Shi, Polyphenol-grafted collagen fiber as reductant and stabilizer for one-step synthesis of size-controlled gold nanoparticles and their catalytic application to 4-nitrophenol reduction, Green Chem. 13 (2011) 651–658, https://doi.org/10.1039/C0GC00843E.

[30] C. Zhang, K. Yu, F. Li, J. Xiang, Acute toxic effects of zinc and mercury on survival, standard metabolism, and metal accumulation in juvenile ridgetail white prawn, Exopalaemon carinicauda, Ecotoxicol. Environ. Saf. 145 (2017) 549–556, https://doi.org/10.1016/j.ecoenv.2017.07.075.

[31] M.M. Cortese, C.V. Suschek, W. Wetzel, K.D. Kroncke, V. Kolb-Bachofen, Zinc protects endothelial cells from hydrogen peroxide via Nrf2-dependent stimulation of glutathione biosynthesis, Free Radic. Biol. Med. 44 (2008) 2002–2012, https://doi.org/10.1016/j.freeradbiomed.2008.02.013.

[32] A. Szuster-Ciesielska, A. Stachura, M. Slotwinska, T. Kaminska, R. Sniezko, R. Paduch, D. Abramczyk, J. Filar, M. Kandefer-Szerszen, The inhibitory effect of zinc on cadmium-induced cell apoptosis and reactive oxygen species (ROS) production in cell cultures, Toxicology 145 (2000) 159–171, https://doi.org/10.1016/s0300-483x(00)00144-x.

[33] D. Zhu, Y. Su, Y. Zheng, B. Fu, L. Tang, Y.X. Qin, Zinc regulates vascular endothelial cell activity through zinc-sensing receptor ZnR/GPR39, Am. J. Physiol. Cell Physiol. 314 (2018) C404–c414, https://doi.org/10.1152/ajpcell.00279.2017.

[34] J. Xiao, S. Chen, J. Yi, H. Zhang, G.A. Ameer, A cooperative copper metal-organic framework-hydrogel system improves wound healing in diabetes, Adv. Funct. Mater. 27 (2017), https://doi.org/10.1002/adfm.201604872.

[35] J. Xiao, Y. Zhu, S. Huddleston, P. Li, B. Xiao, O.K. Farha, G.A. Ameer, Copper metal-organic framework nanoparticles stabilized with folic acid improve wound healing in diabetes, ACS Nano 12 (2018) 1023–1032, https://doi.org/10.1021/acsnano.7b01850.

[36] H. Kim, T. Kawazoe, D.W. Han, K. Matsumara, S. Suzuki, S. Tsutsumi, S.H. Hyon, Enhanced wound healing by an epigallocatechin gallate-incorporated collagen sponge in diabetic mice, Wound Repair Regen. 16 (2008) 714–720, https://doi.org/10.1111/j.1524-475X.2008.00422.x.

[37] M. Kapoor, R. Howard, I. Hall, I. Appleton, Effects of epicatechin gallate on wound healing and scar formation in a full thickness incisional wound healing model in rats, Am. J. Pathol. 165 (2004) 299–307, https://doi.org/10.1016/s0002-9440(10)63297-x.

[38] M. Li, J. Xu, T. Shi, H. Yu, J. Bi, G. Chen, Epigallocatechin-3-gallate augments therapeutic effects of mesenchymal stem cells in skin wound healing, Clin. Exp. Pharmacol. Physiol. 43 (2016) 1115–1124, https://doi.org/10.1111/1440-1681.12652.

[39] P.C. Nagajyothi, S.J. Cha, I.J. Yang, T.V. Sreekanth, K.J. Kim, H.M. Shin, Antioxidant and anti-inflammatory activities of zinc oxide nanoparticles synthesized using Polygala tenuifolia root extract, J. Photochem. Photobiol., B 146 (2015) 10–17, https://doi.org/10.1016/j.jphotobiol.2015.02.008.

[40] E.A. Attia, D.M. Belal, M.H. El Samahy, M.H. El Hamamsy, A pilot trial using topical regular crystalline insulin vs. aqueous zinc solution for uncomplicated cutaneous wound healing: impact on quality of life, Wound Repair Regen. 22 (2014) 52–57, https://doi.org/10.1111/wrr.12122.

[41] S.S. Signorelli, S. Scuto, E. Marino, A. Xourafa, A. Gaudio, Oxidative stress in peripheral arterial disease (PAD) mechanism and biomarkers, Antioxidants (Basel) 8 (2019), https://doi.org/10.3390/antiox8090367.

[42] K. Albrecht-Schgoer, J. Barthelmes, W. Schgoer, M. Theurl, I. Nardin, D. Lener, C. Gutmann, S. Dunnhaupt, A. Bernkop-Schnurch, R. Kirchmair, Nanoparticular delivery system for a secretoneurin derivative induces angiogenesis in a hind limb ischemia model, J. Contr. Release 250 (2017) 1–8, https://doi.org/10.1016/j.jconrel.2017.02.004.

[43] Pipinos II, A.R. Judge, Z. Zhu, J.T. Selsby, S.A. Swanson, J.M. Johanning, B.T. Baxter, T.G. Lynch, S.L. Dodd, Mitochondrial defects and oxidative damage in patients with peripheral arterial disease, Free Radic. Biol. Med. 41 (2006) 262–269, https://doi.org/10.1016/j.freeradbiomed.2006.04.003.

[44] B. Kwon, C. Kang, J. Kim, D. Yoo, B.R. Cho, P.M. Kang, D. Lee, H2O2-responsive antioxidant polymeric nanoparticles as therapeutic agents for peripheral arterial disease, Int. J. Pharm. 511 (2016) 1022–1032, https://doi.org/10.1016/j.ijpharm.2016.08.014.

[45] F. He, L. Zuo, Redox roles of reactive oxygen species in cardiovascular diseases, Int. J. Mol. Sci. 16 (2015) 27770–27780, https://doi.org/10.3390/ijms161126059.

[46] G. Saravanakumar, J. Kim, W.J. Kim, Reactive-oxygen-species-responsive drug delivery systems: promises and challenges, Adv. Sci. (Weinh). 4 (2017) 1600124, https://doi.org/10.1002/advs.201600124.

[47] N. Urao, H. Inomata, M. Razvi, H.W. Kim, K. Wary, R. McKinney, T. Fukai, M. Ushio-Fukai, Role of nox2-based NADPH oxidase in bone marrow and progenitor cell function involved in neovascularization induced by hindlimb ischemia, Circ. Res. 103 (2008) 212–220, https://doi.org/10.1161/circresaha.108.176230.

[48] R. Pan, C. Chen, W.L. Liu, K.J. Liu, Zinc promotes the death of hypoxic astrocytes by upregulating hypoxia-induced hypoxia-inducible factor-1 alpha expression via poly (ADP-ribose) polymerase-1, CNS Neurosci. Ther. 19 (2013) 511–520, https://doi.org/10.1111/cns.12098.